Local structure of Nb in superconducting Nb-doped Bi$_2$Se$_3$

Kirstine Junker Dalgaard [1], Simone Munkholm Kevy,[1] Laura Wollesen [1], Qing Ma [2], Steffen Wiedmann [3],
Kajsa G. V. Sigfridsson Clauss [4], and Martin Bremholm [1,*]

[1]*Department of Chemistry and Interdisciplinary Nanoscience Center, Aarhus University, 8000 Aarhus C, Denmark*
[2]*DND-CAT, Northwestern Synchrotron Research Center at the Advanced Photon Source, Argonne National Laboratory, Argonne, Illinois 60439, USA*
[3]*High Field Magnet Laboratory (HFML-EMFL), Radboud University, 6525 ED Nijmegen, The Netherlands*
[4]*MAX IV Laboratory, Lund University, 22592 Lund, Sweden*

In the prospect of realizing bulk superconductivity in a topological insulator, metal-doped Bi$_2$Se$_3$ has been investigated with increased interest, where the Cu-, Sr-, and Nb-doped systems appear particularly promising. It is generally assumed that metal intercalation into the van der Waals (vdW) gap is responsible for the super-conductivity. We have investigated the local structure of Nb in samples with nominal composition Nb$_{0.25}$Bi$_2$Se$_3$ and Nb$_{0.25}$Bi$_{1.75}$Se$_3$ using the x-ray absorption fine structure technique. It is found that that Nb is primarily located in a local environment consistent with that of the misfit layered structure (BiSe)$_{1+\delta}$NbSe$_2$, which has a δ-dependent superconducting transition in the same temperature range. We explore the possibility of Nb occupancy on various sites in the Bi$_2$Se$_3$ structure, but neither intercalation nor substitution lead to physically meaningful improvements of the models. Furthermore, we report single crystal x-ray diffraction analysis of Nb-doped Bi$_2$Se$_3$. Difference density maps are found to show negligible occupancy in the vdW gap. The misfit layer compound has recently been suggested as an alternative origin for superconductivity in the Nb-doped Bi$_2$Se$_3$ system, in good agreement with the present study. Our findings stress the necessity of thorough structural characterization of these samples. In more general terms, it raises the question of whether metal intercalation is responsible for the superconductivity in the Cu- and Sr-doped Bi$_2$Se$_3$ systems or phase segregation plays a role as well.

I. INTRODUCTION

Topological insulators (TIs) doped with metal atoms have been studied with intense interest in the past decade as a platform for inducing novel physical properties of great interest from a fundamental point of view as well as for novel device fabrication and information technologies [1–3]. This includes magnetic doping and dopant-induced superconductivity [4,5]. Topological superconductors (TSCs) may host non-Abelian Marjorana quasiparticles with potential applications in topological quantum computation [6]. Reported TSC candidates include Bi$_2$Se$_3$ doped with Cu [5,7–10], Sr [11–14], or Nb [15–23]. The electronic properties are closely related to the atomic structure, and thorough structural studies of these systems are therefore important for understanding the origin of doping-induced properties. Previous efforts to map the metal dopant location in M-doped Bi$_2$Se$_3$ (M = Cr, Mn, Fe, Co, Ni, Cu, Nb, Sr) show different dopant structures and dependence on the synthesis method [24–26].

For Cu-, Sr-, and Nb-doped Bi$_2$Se$_3$, metal intercalation between the Bi$_2$Se$_3$ quintuple layers is believed to be driving the superconductivity. This hypothesis was encouraged by reports on electrochemical intercalation of Cu in Bi$_2$Se$_3$, although

further annealing was needed to create superconducting samples [9,27,28]. On the other hand, a study on the local structure of melt-grown Cu$_x$Bi$_2$Se$_3$ suggested Cu substitution on Bi sites in their samples [25]. However, the local structure was not compared with physical property measurements. These deviating findings suggest that the assumption of metal intercalation as the structural origin of the superconductivity may be too simple, and further investigations on the local dopant chemistry of superconducting Bi$_2$Se$_3$ systems are needed.

The Nb$_x$Bi$_2$Se$_3$ system has been reported to contain the misfit layer compound (BiSe)$_{1+\delta}$NbSe$_2$ (typically, $\delta = 0.1$) as an impurity phase [20,23]. This misfit layer compound consists of alternating layers of quasicubic BiSe and NbSe$_2$ [Fig. 1(e)]. The two layer-types have incommensurate periodicity in the a direction, resulting in an incommensurately modulated structure, in short referred to as the *misfit* phase. The misfit phase is in itself superconducting with a transition temperature T_c around 2.4 K [29]. This has been widely overlooked in the literature, and the possibility of a correlation with the superconducting properties of Nb$_x$Bi$_2$Se$_3$, for which the T_c vary between 2.5–3.5 K, has been ignored [20].

Nb$_x$Bi$_2$Se$_3$ is usually synthesized by a melt-growth process followed by quenching the samples at a high temperature (600–650°C). We recently showed that the resulting crystal boules have inhomogeneous composition with multiple phases present: Bi$_2$Se$_3$, trigonal BiSe, and the misfit phase.

*bremholm@chem.au.dk
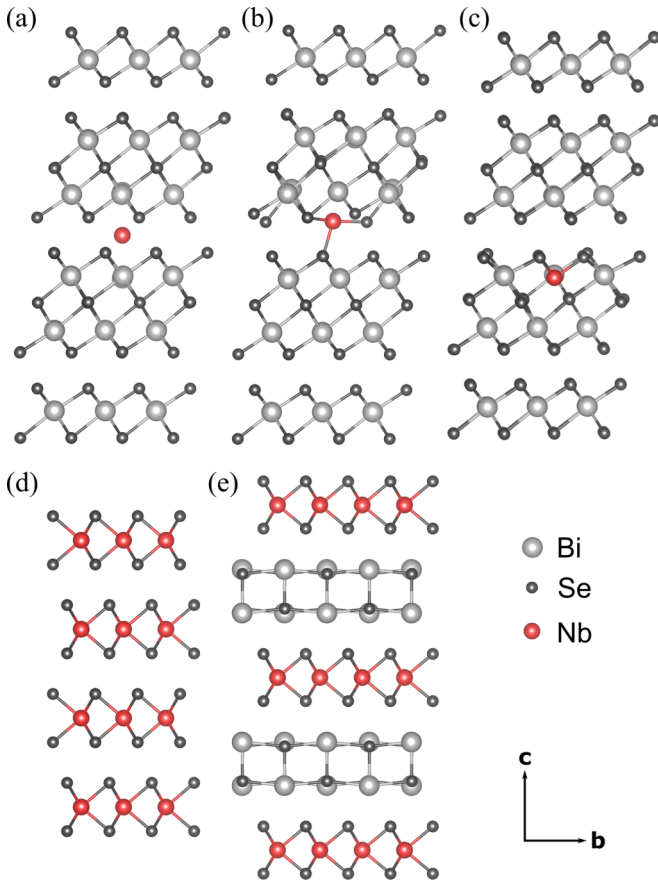
FIG. 1. The DFT relaxed Bi_2Se_3 structures with Nb (a) in interstitial site 1, (b) in interstitial site 2, and (c) substituting for Bi. (d) $NbSe_2$ from Ref. [39]. (e) Schematic of the misfit structure, $(BiSe)_{1+\delta}NbSe_2$ based on the analogous $(BiSe)_{1.1}TaSe_2$ from Ref. [40]. All structures are viewed along their *a* axis.

Furthermore, the phase content and physical properties vary greatly across the crystal boule [30]. The significant phase segregation present in $Nb_xBi_2Se_3$ crystal boules imposes a challenge for identifying the structural origin of the superconductivity. In this study, we investigate the location of Nb dopants in superconducting samples using x-ray absorption fine structure (XAFS) spectroscopy. The analysis shows that Nb is unlikely to be incorporated in the Bi_2Se_3 phase to any significant degree. Rather, it is found to primarily be located in the misfit phase. Our findings are in good agreement with recent reports linking the origin of superconductivity to the presence of the misfit phase [30,31].

II. EXPERIMENTAL

Three crystal boules of Nb-doped Bi_2Se_3 were grown from the pure elements Bi (99.999%), Se (99.999%), and Nb (99.99%) through a melt-growth method described in detail elsewhere [30]. Two of these (C1, C3) were synthesized with nominal stoichiometry $Nb_xBi_2Se_3$ and one (C2) with $Nb_xBi_{2-x}Se_3$, where $x = 0.25$ for all samples. The crystal boules were then divided into different areas of similar size, where the samples S1 (from C1), S2 (from C2), and S3 (from C3) represent a specific area on a crystal boule. An overview

of the specific sample area location and parameters are given in the Supplemental Material [32].

The magnetic susceptibility was measured with a Physical Property Measurement System (PPMS) equipped with a Vibrating Sample Magnetometer in the temperature range 1.8–10 K in a constant 20 Oe field after zero-field-cooling.

The transport experiments were carried out at the High Field Magnet Laboratory (HFML), Nijmegen. Samples were thin flakes of 100–300 μm thickness and of $\sim$1 mm width and $\sim$3 mm length; 25 μm Au wires were attached to the samples with conducting silver paste. Transport experiments were performed in a vacuum tube equipped with an inner vacuum chamber (IVC). Sufficient ^{4}He contact gas was added in the sample space and IVC for measurements at 1.3 K to ensure a good thermal connection. For the temperature sweeps, the IVC was evacuated.

Powder x-ray diffraction (PXRD) measurements were carried out on a Rigaku SmartLab diffractometer with Cu Kα_1 ($\lambda = 1.5406$ Å) radiation in Bragg-Brentano geometry. Single crystal x-ray diffraction (SCXRD) was measured at the BL02B1 beamline ($\lambda = 0.2486$ Å) at SPring-8, Japan. The structure was refined in the program JANA2006 [33].

X-ray absorption spectra at the Nb K-edge were measured at the bending magnet beamline (5-BM-D) of the DND-CAT at the Advanced Photon Source at Argonne National Laboratory, IL, USA (S1 and S2) and the wiggler beamline BALDER at MAX-IV Laboratory, Lund, Sweden (S3). At DND-CAT, a double Si(111) monochromator was used for energy selection with $\Delta E/E = 1.4 \times 10^{-4}$. The x-ray intensities were detuned to 60% of its maximum for harmonic rejection. The samples were held vertically with the x-ray incidence angle at 45°. The measurements of reference spectra were carried out in transmission mode using the spectroscopy-grade ionization chambers (FMB-Oxford). The samples (S1, S2) were measured in fluorescence mode, with the fluorescence signals collected using a 4-element Si-drift solid state detector (Vortex-ME4, Hitachi Corp.) located 90° to the x-ray beam direction. For low-temperature measurements, the Linkam cell (TMHS600, Linkam Scientific, UK) was operated in the liquid cryogenic mode. At BALDER, a LN2 cooled fixed exit double crystal monochromator (FMB Oxford), Si(111) and Si(311), was used for energy selection employing the Si(111) crystals in a continuous scanning scheme [34]. The Nb K-edge spectra of the sample (S3) were measured in fluorescence mode with the sample held vertically with a 55° incidence angle, the so-called *magic angle*, using a 7-element Si-drift solid state detector (X-PIPS, Canberra, Mirion Technologies, Inc., Meriden, CT). Measurements of reference materials were carried out in transmission mode using custom-built ionization chambers (30 cm). Both self-absorption and dead time effects were carefully evaluated and are absent in the data presented here.

The samples for XAFS measurements were fine powders from bulk pieces mixed with a powdered filler, cellulose (for measurements at DND-CAT) or polyethylene (for measurements at BALDER), and cold-pressed into pellets. For S3, no filler was used. The data analysis was performed using the DEMETER software package [35], with the exception that background subtraction from data obtained at BALDER was performed using VIPER [36]. Fitting of the extended x-ray

absorption fine structure (EXAFS) was performed in R-space. In all cases, the atomic distances were constrained to an isotropic expansion or contraction of the model structure, and the coordination numbers were held fixed.

The equilibrium geometry of the candidate interstitial and substitutional models of Nb in Bi_2Se_3 were obtained by standard DFT calculations starting from a $2 \times 2 \times 1$ hexagonal Bi_2Se_3 supercell. We used the plane wave code QUANTUM ESPRESSO [37] and PBEsol ultrasoft pseudopotentials [38]. To simulate the substitutional model, we replaced one Bi ion with Nb. To simulate the interstitial Nb, we placed an Nb atom at different initial coordinates and slightly randomized them, in order to break all spatial symmetries. In all cases, the atomic coordinates and the c axis were fully relaxed.

III. RESULTS

The two candidate Nb-doped Bi_2Se_3 structures, where Nb either occupies the 3b site in the van der Waals (vdW) gap or substitute for Bi, were subject to *ab initio* calculations. This resulted in the two interstitial sites 1 and 2 [Figs. 1(a) and 1(b)] and one substitution site [Fig. 1(c)]. To encourage either an interstitial or a substitution site for Nb, we synthesized samples with both a $Nb_{0.25}Bi_2Se_3$ (S1, S3) and a $Nb_{0.25}Bi_{1.75}Se_3$ (S2) nominal stoichiometry [32]. The samples S1, S2, and S3 investigated here represent a specific area, approximately the middle part, of the three different crystal boules described in the Supplemental Material [32]. Due to the large inhomogeneity of the system, the actual composition is expected to deviate from the nominal.

The PXRD patterns in Fig. 2(a) does indeed reveal that Bi_2Se_3 is the main phase in all three samples, with a small amount of trigonal BiSe in S1. The $(BiSe)_{1+\delta}NbSe_2$ misfit phase is revealed as a minor phase in the PXRD of S1 and S2. For S3, indications of the misfit reflections are visible at the noise level, suggesting $\ll 1\%$ in this sample. For all three samples, the magnetic susceptibility was measured down to 1.8 K [Fig. 2(c)], where only S1 shows a superconducting transition with onset $T_c = 3.1$ K. For S1 and S2, the temperature-dependent resistance was also measured down to 1.4 K [Fig. 2(d)]. S1 shows zero resistance below the transition temperature with onset 3.3 K, in agreement with the susceptibility measurements. A strong decrease in resistance is found for S2 at $T_c = 1.8$ K indicating a transition from a normal state to a superconductor. While some deviation in the onset of superconductivity has been reported for the Nb-doped Bi_2Se_3 system, where a T_c of 2.5 K at present marks the bottom of the interval [41], a transition below 2 K has not been reported before.

To further investigate the location of Nb, SCXRD data were collected for a single crystal from the S2 sample. The inhomogeneity of the system posed a challenge with a high degree of mosaicity, and the layered structure of Bi_2Se_3 makes it prone to twinning and stacking faults. Thus, it required numerous attempts before a suitable crystal was identified. A high-quality data set was only obtained by shooting the focused x-ray beam on the bottom part of a relatively large crystal shown in Fig. 3(a). The x-ray fluorescence spectrum excited above and below the Nb K-edge in Fig. 3(b) was measured for the crystal at the DND-CAT beamline, qualita-
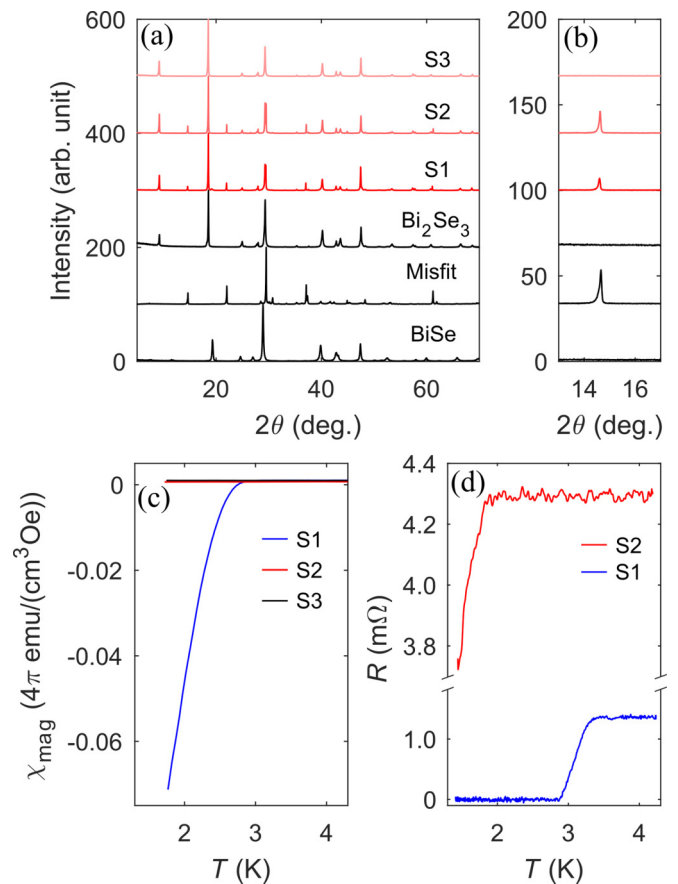
FIG. 2. (a) Powder x-ray diffractograms of the samples S1, S2 and S3 and of synthesized reference materials. In (b), a zoom is shown at the position of the (002) peak of the misfit structure. (c) Magnetic susceptibility of the three samples measured at temperatures down to 1.8 K, at a constant field of 20 Oe. (d) Resistance of S1 and S2 measured down to 1.4 K.

tively confirming the presence of Nb in this particular crystal. A Bi_2Se_3 model was fitted to the data, giving an R-factor of 1.86 (see Supplemental Material for details [32]). The Fourier difference density [Fig. 3(d)] shows a slight excess electron density in the vdW gap with maxima at the 3b sites ($\sim 1 - 2\,e/Å^3$), as well as slight electron deficient Bi and Se sites. While suggestive of intercalation in the vdW gap, the fit was not improved by adding Nb on the 3b site. The apparent low density of $\sim 1\,e/Å^3$ is therefore not caused by any significant Nb $(Z = 41)$ intercalation but ascribed to the fact that small errors tend to accumulate density at high symmetry positions. If Nb was actually present on the 3b site, it would be possible to refine a meaningful nonzero occupancy. The Bi_2Se_3 structure is known to have a tendency to be Se deficient, and fitting the Se occupancy improved the fit slightly. Fluorescence spectroscopy exposing the entire crystal showed the presence of Nb, but given the small size of the x-ray beam required to obtain a high-quality SCXRD data, the Nb content in that specific area of the crystal could differ from the fluorescence average.

The x-ray absorption near-edge structure (XANES) is plotted in Figs. 4(a) and 4(b). There is a resemblance of the XANES between the samples and the misfit phase, which
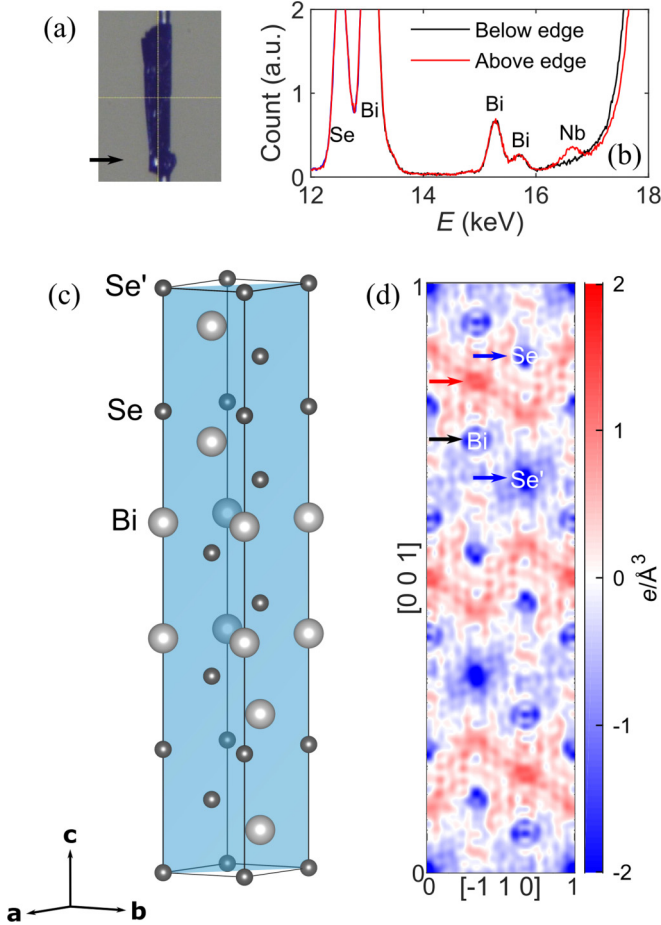
FIG. 3. (a) Image of the S2-crystal for the SCXRD experiment. Only the bottom part, indicated by the arrow, was probed by the beam. (b) Fluorescence spectrum for the whole S2-crystal at 18936 eV (below the Nb K-edge) and at 19036 eV (above the Nb K-edge). (c) Bi_2Se_3 unit cell showing the (110) plane. (d) The Fourier difference electron density of the (110) plane when the SCXRD data were fitted with a Bi_2Se_3 model. Red (blue) indicates excess (deficient) electron density in the data compared with the model. The red arrow shows the 3b site in the vdW gap, the black arrow shows the Bi site, and the two Se sites are indicated by blue arrows.

FIG. 4. XANES spectra of the Nb K-edge measured at 300 K at (a) DND-CAT and (b) BALDER. (c, d) Linear combination fit of the misfit and Nb_2O_5 reference spectra to the S1 (c) and S2 (d) spectrum measured at DND-CAT. (e) Linear combination fit of the misfit and Nb_2O_5 reference spectra to the S3 spectrum measured at BALDER. The fits resulted in the compositions given in the graphs.

decreases in the series: S1, S2, S3. A linear combination fit of the reference spectra gives for S2 and S3 ~2/3 misfit phase and ~1/3 Nb_2O_5, and for S1 ~4/5 misfit phase and ~1/5 Nb_2O_5 [Figs. 4(c)–4(e)]. This apparent presence of Nb_2O_5 should be interpreted with caution. It seems highly unlikely that Nb should be present as an oxide; however, a degree of surface oxidation may play a role. The indication of a strong XANES contribution from the misfit phase for S1 and S2 is in good agreement with the observed peaks in the PXRD pattern. For S3, it is remarkable that the majority of Nb appears to be in the misfit structure, despite barely detectable peak intensity at the expected diffraction angles for this phase in the PXRD. The reason could be that Nb is only present in trace amounts in S3, confirmed by the extended data collection time (~12 h for S3 EXAFS, compared with ~30 min for the $NbSe_2$ standard with similar scan parameters). This is consistent with the misfit phase as the primary Nb-containing

phase in S3. This shows that even for areas with low Nb concentration, the Nb favors to segregate into the misfit phase over intercalation.

Figure 5 shows the EXAFS data $k^2\chi(k)$ and the corresponding Fourier transform moduli $|\chi(R)|$. The EXAFS spectra are dominated by the structure within a single $NbSe_2$ layer, and therefore the misfit phase and $NbSe_2$ EXAFS are not surprisingly very similar. It was thus confirmed by fitting a $NbSe_2$ structural model to the $NbSe_2$ data and misfit data alike that the $NbSe_2$ model can represent the incommensurate misfit phase in our data [32]. The $|\chi(R)|$ of the samples reveal coordination shells with distances that coincide with the coordination shells of a $NbSe_2$ layer in the misfit structure (see the fitted distances in Tables S4 and S5 in the Supplemental Material [32]). However, the amplitudes are smaller, with a decreasing trend in the series S1, S2, S3 when the data measured at the same temperature are compared. A reduced amplitude is in general an indication of a smaller coordination number N or a larger disorder or a combination of both. Since there is a strong resemblance with the $NbSe_2$-type coordination shells, the main structure in the $|\chi(R)|$ of the samples is likely to originate from Nb in the misfit phase, which we consider the main Nb-containing phase. A smaller amount of Nb may be in a different chemical environment, where the
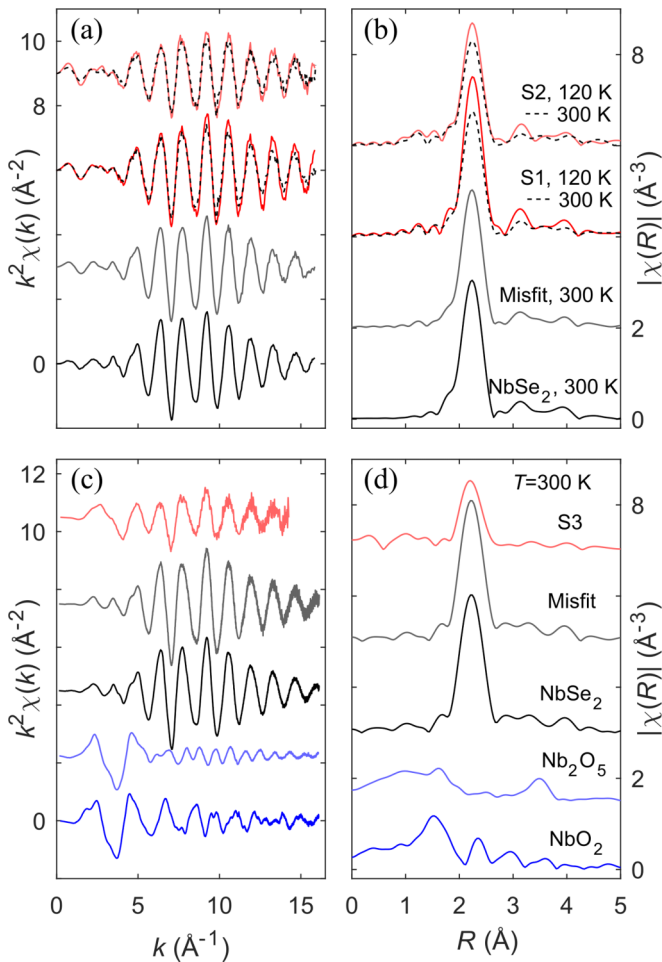
FIG. 5. EXAFS data from (a, b) DND-CAT and (c, d) BALDER plotted as the k^2-weighted $\chi(k)$ and the magnitude of its Fourier transform (FT) $|\chi(R)|$. The FT window 3.15–15 Å^{-1} was used for all spectra in (b), and a window of 3.2–13.0 Å^{-1} was used for S3, the misfit phase reference and NbSe$_2$ in (d). A window of 2.9–15.2 Å^{-1} was used for the NbO$_2$ and Nb$_2$O$_5$. The labels in (b) and (d) are the same for graphs of the same color in (a) and (c), respectively. For S1 and S2, the solid line indicates the low temperature, and the dashed line indicates the 300 K data.

small amplitude contribution at ~1.5 Å in the $|\chi(R)|$ suggests a chemical environment of low-Z atoms. We will return to this issue in the Discussion.

The EXAFS data were fitted using the NbSe$_2$ structural model, which here represents the misfit phase. The fit was performed with either a fixed amplitude reduction factor of $S_0^2 = 1.0$ obtained from the NbSe$_2$ standard [32] or with S_0^2 as fitting parameter. The results are plotted in Figs. 6(a)–6(b), and the fitted parameters are given in Tables I–III. A marked reduction in the R-factor is achieved for all three samples when S_0^2 is fitted. The variable S_0^2 parameters also bring about a reduction in disorder parameters σ^2, which then assume values closer to what may be expected at the given temperatures. The reduction in S_0^2 from the standard value of 1.0 represents an adjustment of the coordination numbers, a misfit phase fraction below 1, or both. Note that the fitted S_0^2 for the three samples follow the trend of the XANES linear combination fits in Figs. 4(c)–4(e). For S1 and S2, the room
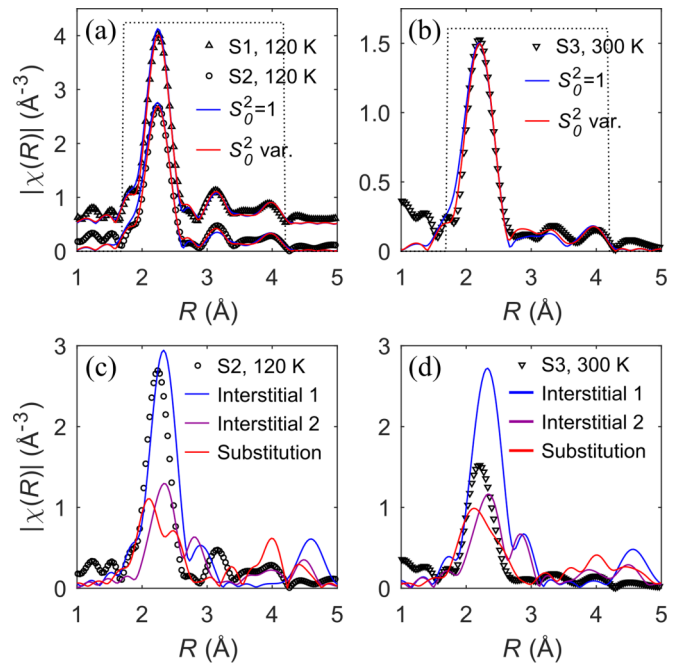
FIG. 6. (a, b) The NbSe$_2$ (representing the misfit layer compound) model fitted to the EXAFS data of (a) S1 plotted with an upward shift and S2, and (b) S3. The amplitude reduction factor was either fixed to $S_0^2 = 1.0$ (blue line) or a fitted variable (red line). (c, d) The magnitude of $\chi(R)$ of the DFT relaxed structures in Figs. 1(a)–1(c) along with the measured EXAFS for S2 (c) and S3 (d). The DFT models were not fitted to the data but plotted with the same user-defined σ^2 for all single-scattering paths in all models. A FT window of 3.15–15.0 Å^{-1} was used in (a, c) and 3.2-13.0 Å^{-1} in (b, d).

temperature data were fitted using the same model and with results similar to those obtained for the low-temperature data, except for the disorder parameters. These are given in square brackets in Tables I and II for comparison. It is noteworthy that although the disorder parameters for S1 and S2 are similar at room temperature, the reduction in σ^2 on cooling is greater for S1. Thus, thermal vibration is more significant in S1, and static disorder dominates in S2. In other words, S1 has a much more ordered local structure around Nb.

We also considered the EXAFS of the proposed *ab initio* models of Nb-doped Bi$_2$Se$_3$ in Figs. 1(a)–1(c), plotted with user-defined σ^2 in Figs. 6(c) and 6(d). These model structures do not describe the EXAFS data of the samples well. However, we did perform linear combination fits to the S3 EXAFS data including the NbSe$_2$ model with fixed parameters and each of the DFT relaxed structure models (see Supplemental Material for details [32]). The inclusion of either of the three DFT models did not improve the fit, unless the σ^2 were allowed to assume unreasonably large values. This suggests that Nb-doped Bi$_2$Se$_3$ corresponding to the models shown in Figs. 1(a)–1(c) are at most present as minor contributions to the Nb K-edge signal.

IV. DISCUSSION

The present study was initially intended as an effort to locate Nb dopants in superconducting Nb$_x$Bi$_2$Se$_3$ and

TABLE I. Fitted EXAFS parameters. Sample: S1; $T \approx 120$ K; Model: $NbSe_2$; R-range: 1.7–4.2 Å; k-range: 3.15–15.0 Å^{-1}. The σ^2 for a similar fit at $T = 300$ K are given in brackets for comparison. The given uncertainties are from the least-squares fitting; however, the spatial resolution is ~0.01 Å.

Path	N	R (Å)	σ^2 (Å^2)	S_0^2	ΔE_0 (eV)	R_f (%)	Variables/ independent points
			Fixed S_0^2				
Se1	6	2.60(0)	0.0036(2) [0.0050(2)]				
Nb1	6	3.45(1)	0.0108(18) [0.016(4)]	1	−0.4(1.0)	2.1	5/18.4
Se2	6	4.32(1)	0.009(3) [0.013(4)]				
Se1-Nb1	24	4.32(1)	σ^2(Se1)+σ^2(Nb1)				
			Variable S_0^2				
Se1	6	2.60(0)	0.0024(3) [0.0037(4)]				
Nb1	6	3.45(0)	0.0091(12) [0.013(2)]	0.77(5)	−0.4(7)	0.81	6/18.4
Se2	6	4.32(0)	0.0079(17) [0.011(3)]				
Se1-Nb1	24	4.32(0)	σ^2(Se1)+σ^2(Nb1)				

$Nb_xBi_{2-x}Se_3$ samples. This is particularly challenging, since a synthesis route leading to highly heterogeneous samples is necessary to obtain the desired superconducting properties. No superconducting area of a synthesized crystal boule that was also phase pure Bi_2Se_3 was identified. Thus, the experiments were carried out on samples with varying, but small, amounts of the misfit phase. From the XAFS data, the misfit structure appears to be the main Nb-containing phase in all samples, although the amplitudes of the EXAFS oscillations

are reduced with respect to the misfit reference data. There can be several, possibly simultaneous, reasons for this. The most apparent reason would be a lower coordination number of Nb due to Se vacancies. Chalcogenide vacancies are common in transition metal dichalcogenides [42–44], and it is likely that they form in the $NbSe_2$ layer of the misfit phase as well, especially considering that the misfit phase is formed in a Nb-doped Bi_2Se_3 matrix with high-temperature quenching. This would explain why the misfit and $NbSe_2$ reference samples

TABLE II. Fitted EXAFS parameters. Sample: S2; $T \approx 120$ K; Model: $NbSe_2$; R-range: 1.7–4.2 Å; k-range: 3.15–15.0 Å^{-1}. The σ^2 for a similar fit at $T = 300$ K are given in brackets for comparison. The given uncertainties are from the least-squares fitting; however, the spatial resolution is ~0.01 Å.

Path	N	R (Å)	σ^2 (Å^2)	S_0^2	ΔE_0 (eV)	R_f (%)	Variables/ independent points
			Fixed S_0^2				
Se1	6	2.60(1)	0.0051(3) [0.0061(4)]				
Nb1	6	3.45(1)	0.014(4) [0.021(8)]	1	−0.7(1.4)	4.8	5/18.4
Se2	6	4.32(1)	0.010(4) [0.012(5)]				
Se1-Nb1	24	4.32(1)	σ^2(Se1)+σ^2(Nb1)				
			Variable S_0^2				
Se1	6	2.60(0)	0.0030(4) [0.0040(5)]				
Nb1	6	3.44(0)	0.0104(17) [0.014(3)]	0.66(5)	−0.7(9)	1.3	6/18.4
Se2	6	4.31(1)	0.008(2) [0.010(3)]				
Se1-Nb1	24	4.32(1)	σ^2(Se1)+σ^2(Nb1)				

TABLE III. Fitted EXAFS parameters. Sample: S3; $T = 300$ K; Model: NbSe$_2$; R-range: 1.7–4.2 Å; k-range: 3.2–13.0 Å^{-1}. The given uncertainties are from the least-squares fitting; however, the spatial resolution is ~0.01 Å.

Path	N	R (Å)	σ^2 (Å^2)	S_0^2	ΔE_0 (eV)	R_f (%)	Variables/ independent points
			Fixed S_0^2				
Se1	6	2.60(1)	0.0087(6)				
Nb1	6	3.44(1)	0.022(8)	1	−2.7(1.9)	6.8	5/15.2
Se2	6	4.31(2)	0.015(6)				
Se1-Nb1	24	4.32(2)	σ^2(Se1)+σ^2(Nb1)				
			Variable S_0^2				
Se1	6	2.60(1)	0.0055(9)				
Nb1	6	3.44(1)	0.015(4)	0.62(9)	−2.5(1.6)	2.6	6/15.2
Se2	6	4.31(1)	0.012(5)				
Se1-Nb1	24	4.31(1)	σ^2(Se1)+σ^2(Nb1)				

do not display similar amplitude reduction. An abundance of Se-vacancies could lead to the formation of Nb-O bonds in the fine-grained powder, explaining the small peak at low R in the $|\chi(R)|$ and the apparent oxide contribution in the XANES. Few- or single-layer NbSe$_2$ is known to degrade in air over time [45], suggesting that defective NbSe$_2$ surface layers in the misfit phase could also be sensitive to air exposure.

An *ab initio* study on the related misfit layer compound (PbS)$_{1.14}$TaS$_2$ showed a stabilizing effect of Ta substitution on Pb sites [46]. Similarly, Nb substitution on Bi sites may stabilize the (BiSe)$_{1+\delta}$NbSe$_2$ in our samples. In that case, it would give a reduction in the Nb coordination number, as Bi is only coordinated to five Se in the quasicubic BiSe layer.

As previously mentioned, the harsh synthesis conditions may have produced a distribution of misfit stoichiometries, which will add significant structural disorder effects in the EXAFS. Variation of δ in (BiSe)$_{1+\delta}$NbSe$_2$ is discussed later in this section.

Despite the lack of clarity on the origin of the reduced amplitude of the EXAFS oscillations, the sum of the evidence suggests a strong tendency toward the formation of the misfit phase rather than incorporation of Nb dopants into the Bi$_2$Se$_3$ host structure. In a recent study [30], we estimated that the total phase content across a crystal boule (from which S1 originates) fits approximately with the assumption that all or most of the Nb in the synthesis appear in the misfit phase. We also found that all superconducting samples contained this phase. Another recent study found a correlation between the superconducting volume fraction and the amount of (BiSe)$_{1+\delta}$NbSe$_2$ in Nb-doped Bi$_2$Se$_3$ samples [31]. These authors suggested that Nb doping in the Bi$_2$Se$_3$ phase does not take place, and that the origin of superconductivity in "Nb$_x$Bi$_2$Se$_3$" samples is to be found in the presence of the misfit phase. Thus, we find it relevant to reevaluate the role of this structure in superconducting samples of composition Nb$_x$Bi$_2$Se$_3$ or Nb$_x$Bi$_{2-x}$Se$_3$.

(BiSe)$_{1+\delta}$NbSe$_2$ was first reported as BiNbSe$_3$ by Gotoh *et al.* in 1989 [47] and then by Zhou *et al.* in 1992 [40] for $\delta = 0.10$; a few years later, Nader *et al.* [29] reported superconductivity with a T_c of ~2.4 K. In general, misfit-layered compounds $(MX)_{1+\delta}(TX_2)_m$ ($m = 1, 2$ or 3; $M = $ Pb, Sn,

Bi, rare earth; $T = $ Ta, Nb; $X = $ S, Se) have values of δ in the range $0.08 < \delta < 0.23$. Perfectly stoichiometric cases will have a specific value of δ, and for (BiSe)$_{1+\delta}$NbSe$_2$, this value is $\delta = 0.1$. Recently, Nagao *et al.* [48] showed that large variations in the stoichiometry are possible, and that the superconducting transition temperature is varied in response. They found a T_c of 2.4 K for $\delta = 0$ and 3.2 K for $\delta = 0.33$ (the latter was reported as Nb$_{0.9}$Bi$_{1.2}$Se$_3$). This range of T_c overlaps well with the variation in critical temperature typically observed in superconducting Nb$_x$Bi$_2$Se$_3$ samples. A similar variation in stoichiometry and superconducting transition temperature has been suggested for other misfit layer compounds [29,49]. Thus, we may understand the variation in T_c in Nb$_x$Bi$_2$Se$_3$ systems as compositional variations in the misfit impurity phase, which may induce the superconductivity through a proximity effect. Such a variation can be expected in real materials formed in an off-stoichiometric matrix where multiple phases coexist. Further deviations can be expected when high temperature quenching is done.

The T_c of 3.3 K for S1 in our study falls within the typically observed range, while the transition at 1.8 K of S2 has not been reported before. Others may have made samples with a similar low-temperature transition but failed to discover it, since a typical PPMS has a lower temperature limit around 1.8 K.

The reduced Bi content in the S2 synthesis may have encouraged a smaller value of δ in the misfit phase. A smaller value of δ gives a smaller T_c according to Nagao *et al.* [48]. However, it remains an unanswered question whether a variation in the misfit stoichiometry, disorder, or defect structure can bring about a reduction in the T_c as significant as the one we report for S2. It should also be noted that the synthesis conditions employed for the pure misfit phase [29,31,40] is vastly different from the conditions in which the misfit phase is formed in superconducting Nb$_x$Bi$_2$Se$_3$ or Nb$_x$Bi$_{2-x}$Se$_3$ samples. Thus, the range of T_c achievable in a misfit phase may be wider than suggested by the literature to date.

For S3, the insignificant misfit content may be the reason for the lack of a superconducting transition above 1.8 K, making the superconducting proximity too weak for detection.

V. CONCLUSION

We have synthesized and characterized samples of Nb-doped Bi_2Se_3 to investigate the link between structure and superconductivity in this system. In agreement with previous reports, one sample from a crystal boule of nominal content $Nb_{0.25}Bi_2Se_3$ showed a superconducting transition at $T_c = 3.3$ K. Another sample from a crystal boule of nominal content $Nb_{0.25}Bi_{1.75}Se_3$ showed indication of a superconducting transition at 1.8 K, which has not been reported before. The investigations of the local structure with XAFS as the primary technique indicate a strong preference for Nb to be in the superconducting misfit layer compound $(BiSe)_{1+\delta}NbSe_2$, even for low dopant concentrations. Nb did not appear to incorporate into the Bi_2Se_3 phase to any significant degree. This finding is in agreement with recent reports where the presence of the misfit phase is offered as an alternative origin of superconductivity in Nb-doped Bi_2Se_3.

[1] L. Fu and E. Berg, Phys. Rev. Lett. **105**, 097001 (2010).

[2] Y. L. Chen, J.-H. Chu, J. G. Analytis, Z. K. Liu, K. Igarashi, H.-H. Kuo, X. L. Qi, S. K. Mo, R. G. Moore, D. H. Lu *et al.*, Science **329**, 659 (2010).

[3] Y. Tokura, K. Yasuda, and A. Tsukazaki, Nat. Rev. Phys. **1**, 126 (2019).

[4] R. Yu, W. Zhang, H.-J. Zhang, S.-C. Zhang, X. Dai, and Z. Fang, Science **329**, 61 (2010).

[5] L. A. Wray, S.-Y. Xu, Y. Xia, Y. S. Hor, D. Qian, A. V. Fedorov, H. Lin, A. Bansil, R. J. Cava, and M. Z. Hasan, Nat. Phys. **6**, 855 (2010).

[6] A. Kitaev, Ann. Phys. **303**, 2 (2003).

[7] Y. S. Hor, A. J. Williams, J. G. Checkelsky, P. Roushan, J. Seo, Q. Xu, H. W. Zandbergen, A. Yazdani, N. P. Ong, and R. J. Cava, Phys. Rev. Lett. **104**, 057001 (2010).

[8] S. Sasaki, M. Kriener, K. Segawa, K. Yada, Y. Tanaka, M. Sato, and Y. Ando, Phys. Rev. Lett. **107**, 217001 (2011).

[9] M. Kriener, K. Segawa, Z. Ren, S. Sasaki, S. Wada, S. Kuwabata, and Y. Ando, Phys. Rev. B **84**, 054513 (2011).

[10] J. A. Schneeloch, R. D. Zhong, Z. J. Xu, G. D. Gu, and J. M. Tranquada, Phys. Rev. B **91**, 144506 (2015).

[11] Z. Liu, X. Yao, J. Shao, M. Zuo, L. Pi, S. Tan, C. Zhang, and Y. Zhang, J. Am. Chem. Soc. **137**, 10512 (2015).

[12] Y. Pan, A. M. Nikitin, G. K. Araizi, Y. K. Huang, Y. Matsushita, T. Naka, and A. de Visser, Sci. Rep. **6**, 28632 (2016).

[13] A. Y. Kuntsevich, M. A. Bryzgalov, V. A. Prudkoglyad, V. P. Martovitskii, Y. G. Selivanov, and E. G. Chizhevskii, New J. Phys. **20**, 103022 (2018).

[14] H. Leng, D. Cherian, Y. K. Huang, J.-C. Orain, A. Amato, and A. de Visser, Phys. Rev. B **97**, 054503 (2018).

[15] Y. Qiu, K. Nocona Sanders, J. Dai, J. E. Medvedeva, W. Wu, P. Ghaemi, T. Vojta, and Y. San Hor, arXiv:1512.03519 (2015).

[16] B. J. Lawson, P. Corbae, G. Li, F. Yu, T. Asaba, C. Tinsman, Y. Qiu, J. E. Medvedeva, Y. S. Hor, and L. Li, Phys. Rev. B **94**, 041114(R) (2016).

[17] M. P. Smylie, H. Claus, U. Welp, W.-K. Kwok, Y. Qiu, Y. S. Hor, and A. Snezhko, Phys. Rev. B **94**, 180510(R) (2016).

[18] M. P. Smylie, K. Willa, H. Claus, A. Snezhko, I. Martin, W.-K. Kwok, Y. Qiu, Y. S. Hor, E. Bokari, P. Niraula *et al.*, Phys. Rev. B **96**, 115145 (2017).

[19] T. Asaba, B. J. Lawson, C. Tinsman, L. Chen, P. Corbae, G. Li, Y. Qiu, Y. S. Hor, L. Fu, and L. Li, Phys. Rev. X **7**, 011009 (2017).

[20] K. Kobayashi, T. Ueno, H. Fujiwara, T. Yokoya, and J. Akimitsu, Phys. Rev. B **95**, 180503(R) (2017).

[21] A. Sirohi, S. Das, P. Neha, K. S. Jat, S. Patnaik, and G. Sheet, Phys. Rev. B **98**, 094523 (2018).

[22] C. Kurter, A. D. K. Finck, E. D. Huemiller, J. Medvedeva, A. Weis, J. M. Atkinson, Y. Qiu, L. Shen, S. H. Lee, T. Vojta *et al.*, Nano Lett. **19**, 38 (2018).

[23] J. Wang, F. Jiao, D. Zhang, M. Chang, L. Cai, Y. Li, C. Wang, S. Tan, Q. Jing, B. Liu *et al.*, J. Phys. Chem. Solids **137**, 109208 (2020).

[24] A. I. Figueroa, G. van der Laan, L. J. Collins-McIntyre, G. Cibin, A. J. Dent, and T. Hesjedal, J. Phys. Chem. C **119**, 17344 (2015).

[25] Z. Liu, X. Wei, J. Wang, H. Pan, F. Ji, F. Xi, J. Zhang, T. Hu, S. Zhang, Z. Jiang *et al.*, Phys. Rev. B **90**, 094107 (2014).

[26] Z. Li, M. Wang, D. Zhang, N. Feng, W. Jiang, C. Han, W. Chen, M. Ye, C. Gao, J. Jia *et al.*, Phys. Rev. Mater. **2**, 014201 (2018).

[27] T. Shirasawa, M. Sugiki, T. Hirahara, M. Aitani, T. Shirai, S. Hasegawa, and T. Takahashi, Phys. Rev. B **89**, 195311 (2014).

[28] J. Zhang, J. Sun, Y. Li, F. Shi, and Y. Cui, Nano Lett. **17**, 1741 (2017).

[29] A. Nader, A. Briggs, and Y. Gotoh, Solid State Commun. **101**, 149 (1997).

[30] S. M. Kevy, H. E. Lund, L. Wollesen, K. J. Dalgaard, Y.-T. Hsu, S. Wiedmann, M. Bianchi, A. J. U. Holt, D. Curcio, D. Biswas, A. J. H. Jones, K. Volckaert, C. Cacho, P. Dudin, P. Hofmann, M. Bremholm, Phys. Rev. B **103**, 085107 (2021).

[31] M. E. Kamminga, M. Batuk, J. Hadermann, and S. J. Clarke, Commun. Mater. **1**, 82 (2020).

[32] See Supplemental Material at http://link.aps.org/supplemental/10.1103/PhysRevB.103.184103 for additional experimental details and data analysis; including Ref. [33,50–53].

[33] V. Petříček, M. Dušek, and L. Palatinus, Z. Kristallogr. - Cryst. Mater. **229**, 345 (2014).

[34] I. Persson, D. Lundberg, É. G. Bajnóczi, K. Klementiev, J. Just, and K. G. V. Sigfridsson Clauss, Inorg. Chem. **59**, 9538 (2020).

[35] B. Ravel and M. Newville, J. Synchrotron Radiat. **12**, 537 (2005).

[36] K. V. Klementev, J. Phys. D: Appl. Phys. **34**, 209 (2000).

[37] P. Giannozzi, S. Baroni, N. Bonini, M. Calandra, R. Car, C. Cavazzoni, D. Ceresoli, G. L. Chiarotti, M. Cococcioni, I. Dabo *et al.*, J. Phys.: Condens. Matter **21**, 395502 (2009).

[38] K. F. Garrity, J. W. Bennett, K. M. Rabe, and D. Vanderbilt, Comput. Mater. Sci. **81**, 446 (2014).

[39] V. L. Kalikhman, Izv. Akad. Nauk SSSR, Neorg. Mater. **19**, 1060 (1983).

[40] W. Zhou, A. Meetsma, J. de Boer, and G. Wiegers, Mater. Res. Bull. **27**, 563 (1992).

[41] M. M. Sharma, P. Rani, L. Sang, X. L. Wang, and V. P. S. Awana, J. Supercond. Novel Magn. **33**, 565 (2020).

[42] O. N. Andreeva, I. S. Braude, and A. A. Mamalui, Phys. Met. Metallogr. **113**, 888 (2012).

[43] Z. Lin, B. R. Carvalho, E. Kahn, R. Lv, R. Rao, H. Terrones, M. A. Pimenta, and M. Terrones, 2D Mater. **3**, 022002 (2016).

[44] P. Manchanda and R. Skomski, Superlattices Microstruct. **101**, 349 (2017).

[45] Y. Cao, A. Mishchenko, G. L. Yu, E. Khestanova, A. P. Rooney, E. Prestat, A. V. Kretinin, P. Blake, M. B. Shalom, C. Woods *et al.*, Nano Lett. **15**, 4914 (2015).

[46] E. Kabliman, P. Blaha, and K. Schwarz, Phys. Rev. B **82**, 125308 (2010).

[47] Y. Gotoh, M. Onoda, K. Uchida, Y. Tanaka, T. Iida, H. Hayakawa, and Y. Oosawa, Chem. Lett. **18**, 1559 (1989).

[48] M. Nagao, A. Miura, Y. Horibe, Y. Maruyama, S. Watauchi, Y. Takano, and I. Tanaka, Solid State Commun. **321**, 114051 (2020).

[49] Y. Moelo, A. Meerschaut, J. Rouxel, and C. Auriel, Chem. Mater. **7**, 1759 (1995).

[50] L. Krause, K. Tolborg, T. B. E. Grønbech, K. Sugimoto, B. B. Iversen, and J. Overgaard, J. Appl. Crystallogr. **53**, 635 (2020).

[51] Bruker, SAINT-Plus Integration Engine, Version 8.38A, Bruker AXS Inc., Madison, Wisconsin, USA, 2013.

[52] L. Krause, R. Herbst-Irmer, G. M. Sheldrick, and D. Stalke, J. Appl. Crystallogr. **48**, 3 (2015).

[53] R. H. Blessing, J. Appl. Crystallogr. **30**, 421 (1997).